PCCP

Accepted Manuscript

This is an *Accepted Manuscript*, which has been through the Royal Society of Chemistry peer review process and has been accepted for publication.

Accepted Manuscripts are published online shortly after acceptance, before technical editing, formatting and proof reading. Using this free service, authors can make their results available to the community, in citable form, before we publish the edited article. We will replace this *Accepted Manuscript* with the edited and formatted *Advance Article* as soon as it is available.

You can find more information about *Accepted Manuscripts* in the **Information for Authors**.

Please note that technical editing may introduce minor changes to the text and/or graphics, which may alter content. The journal's standard **Terms & Conditions** and the **Ethical guidelines** still apply. In no event shall the Royal Society of Chemistry be held responsible for any errors or omissions in this *Accepted Manuscript* or any consequences arising from the use of any information it contains.

Journal Name

ARTICLE

Selective Electrochemical Reduction of CO_2 to CO on CuO-derived Cu Nanowires†

Ming Ma,[a] Kristina Djanashvili[b] and Wilson A. Smith*[,a]

In this work, we report a new synthesis method to prepare a Cu nanowire electrocatalyst for selective CO_2 reduction at room temperature and atmospheric pressure. Cu nanowire array electrodes were prepared through a two-step synthesis of $Cu(OH)_2$ and CuO nanowire arrays on Cu foil substrates and a subsequent electrochemical reduction of the CuO nanowire arrays. The Cu nanowire arrays are able to electrochemically reduce CO_2 to CO with a faradaic efficiency of ~50% at a moderate overpotential of 490 mV, which is significantly higher than that of polycrystalline Cu foil catalysts at identical conditions. The improved faradaic efficiency for the reduction of CO_2 to CO is ascribed to the enhanced stabilization for the CO_2*^- intermediate on the high surface area Cu nanowire arrays.

1. Introduction

The increasing global CO_2 concentration is a serious environmental threat that is responsible for climate change[1] and ocean acidification[2]. To reduce anthropogenic CO_2 emissions into the atmosphere, the capture and sequestration of CO_2 at large emission sources such as industrial power plants has been proposed.[3,4] However, sequestration methods including geological and deep sea storage has some unknown ecological and environmental impacts and risk. For the utilization of the captured CO_2, the electrochemical reduction of CO_2 has attracted considerable attention as an attractive solution.[4–14] In this process, CO_2 could be employed as a chemical feedstock and converted into high energy density fuels such as syngas (carbon monoxide (CO) and hydrogen) and other hydrocarbons.[7–9] In order to avoid extra CO_2 emission, the process of the electrochemical reduction of CO_2 can be coupled to renewable energy sources such as solar energy, wind energy and hydropower.[4,7]

The selective electrochemical reduction of CO_2 to CO at room temperature is a particularly interesting reaction, which can be a potential key step in the development of a clean and sustainable energy supply. Traditionally, CO is produced at an industrial scale from a wide variety of materials that includes natural gas, residual oil, petroleum coke and coal.[15] CO can be used as chemical feedstock in the Fischer–Tropsch process, a well-developed technology that has been used in industry to generate chemicals (such as methanol) and synthetic fuels (such as diesel fuel) from syngas (CO and H_2) for many decades.[4,5] A key technological challenge for the electroreduction of CO_2 to CO is to develop a suitable catalyst that is capable of achieving a stable and cost-effective process with high efficiency and selectivity at low overpotentials.[5,7,16–18]

Researchers have investigated the electrochemical reduction of CO_2 using various metal electrodes in CO_2-saturated aqueous solutions at ambient temperature.[4–10,16–24] As many as 16 different products have been reported from the electroreduction of CO_2,[7] thus it is necessary to find catalyst materials with a high selectivity towards a desired product formation. It has been demonstrated that polycrystalline Au and Ag are capable of reducing CO_2 to CO with high efficiency in CO_2-saturated aqueous electrolytes.[6,9,19,21] However, Au and Ag are not suitable catalyst materials for large-scale applications due to their high cost and low abundance. Developing cheap and earth-abundant catalysts with a simple and scalable method for fabrication and high selectivity for CO production is essential for achieving large-scale utilization of CO_2 reduction.

The focus of most CO_2 reduction studies has concentrated on Cu electrodes because Cu is capable of reducing CO_2 to CO and hydrocarbons such as CH_4 and C_2H_4, in CO_2 saturated-aqueous electrolytes at ambient pressure and temperature, as first reported by Y. Hori.[25,26] It has been demonstrated that the surface morphology and roughness of copper electrodes have a dramatic influence on the catalytic activity and product selectivity during the electrochemical reduction of CO_2.[10,18,27–29] Tang et al. reported that Cu nanoparticle covered electrodes showed better selectivity towards ethylene and CO formation

[a.] Materials for Energy Conversion and Storage, Department of Chemical Engineering, Faculty of Applied Sciences, Delft University of Technology, P.O. Box 5045, 2600 GA Delft, The Netherlands Address here.
[b.] Biocatalysis, Department of Biotechnology, Faculty of Applied Sciences, Delft University of Technology, P.O. Box 5045, 2600 GA Delft, The Netherlands
* Author to whom correspondence should be addressed. E-mail address: W.A.Smith@tudelft.nl   Tel.: +31 15 27 82659; Fax: +31 15 27 87421.
† Electronic Supplementary Information (ESI) available: See DOI: 10.1039/x0xx00000x

compared with the other two electrodes, an electropolished Cu electrode and an argon gas sputtered Cu electrode.[29] In that study, the improvement in CO_2 reduction performance was explained by the high surface area which was able to provide a greater abundance of undercoordinated sites on the roughened Cu surface.[29] Kanan *et al.* have shown that a modified Cu electrode (thick Cu_2O film-derived Cu) prepared by annealing Cu foil in air at 500 ºC for 12 h has a large roughness factor, resulting in a very high selectivity for CO formation at low potentials, though the exact mechanism for the improved selectivity was not well established.[18] In addition, it was reported that Cu nanofoams exhibited a better selectivity to HCOOH production compared to polycrystalline Cu during electrochemical CO_2 reduction.[10] Recently, the effect of the size of Cu nanoparticles on CO_2 electroreduction has been demonstrated, showing an increase in the catalytic activity and selectivity for CO and H_2 with decreasing Cu particle size.[27] All the above studies indicate that a nanostructured surface morphology has a significant effect on the catalytic activity and selectivity for the electrochemical reduction of CO_2. However, there is little reported research on high surface area Cu nanowires for electrochemical reduction of CO_2.[18,30]

Here, we show the first example of the electrochemical reduction of CO_2 on Cu nanowires reduced from CuO with a simple fabrication method. The Cu nanowire arrays are able to electrochemically reduce CO_2 to different products, with a predominant formation of CO with a significantly higher faradaic efficiency (FE) than polycrystalline Cu at moderate overpotentials (η < 500 mV). Compared to the Cu electrode prepared by annealing Cu foil in air at 500 ºC for 12 h (FE for CO is ~45% at η < 390 mV)[18], the Cu nanowire arrays prepared at 150 ºC for 2 h has a comparable FE of ~50% for CO production at a moderate overpotential (η = 490 mV). Furthermore, a Tafel plot for the Cu nanowires prepared by a simple synthesis method was found to have a slope of ~110 mV/dec at low overpotential (η < 0.3 V), which is consistent with that (116 mV/dec) of Cu electrodes prepared at 500 ºC for 12 h,[18] implying a favorable formation of the CO_2^{*-} intermediate while suppressing hydrogen evolution. Therefore, this study shows that an easily fabricated CuO-derived Cu nanowire array offers a highly selective platform for the electrochemical reduction of CO_2 to CO.

2. Experimental section

2.1 Fabrication of CuO Nanowires

$Cu(OH)_2$ nanowires were first synthesized on Cu foils using a simple wet chemical method.[31,32] The Cu foils were ultrasonically cleaned in acetone and ethanol and then rinsed with de-ionized water. The cleaned Cu foils were dried with nitrogen and then immersed into a solution mixture containing 0.133 M $(NH_4)_2S_2O_8$ and 2.667 M NaOH for 15 min. After this time the Cu foils turned a deep blue color (the blue color is indicative of the formation of $Cu(OH)_2$ nanowires.[31]) and were taken out from the solution, rinsed with de-ionized water and

absolute ethanol, and dried with nitrogen. After that, CuO nanowires were fabricated by annealing the $Cu(OH)_2$ nanowire arrays at 150 ºC for 2 hours under an air atmosphere.

2.2 Physical Characterization

The morphology and nanostructure of the samples before and after electrochemical reduction of CO_2 were characterized by using scanning electron microscope (SEM, JEOL JSM-6010LA). The crystal structure of the samples was measured by X-ray diffraction (XRD) using a diffractometer (Bruker AXS GmbH-D8 Discover) with Co-Kα radiation (λ = 1.7903 Å). X-ray photoelectron spectroscopy (XPS, Thermo Scientific™ K-Alpha™) was used to confirm the oxidation states of Cu in the samples before and after the electrolysis.

2.3 Surface Area Measurements

Surface roughness factors of the Cu nanowires and polycrystalline Cu foils were determined by measuring electrochemical double-layer capacitance.[28,33,34] The cyclic voltammograms (CVs) were measured in N_2 bubbled 0.1 M phosphate buffer for a potential range in which no faradaic processes were occurring (Fig. S6 and Fig. S7). The geometric current density (j_{tot}) was plotted against the scan rate of the CV and the slope of the linear regression was used to determine the capacitance (C). The surface roughness factor can be obtained by normalizing the capacitance value to that of polycrystalline Cu foil (the surface roughness factor of polycrystalline Cu is used as the standard reference)

2.4 Electrochemical CO_2 Reduction

CO_2 electrolysis experiments were performed in an electrochemical cell made from Teflon (Fig. 1) using a three electrode configuration at ambient temperature and pressure. The cell consists of two compartments (working and counter electrode compartments), which is separated by a Nafion-115 proton exchange membrane to prevent the oxidation of CO_2 reduction products. In the three-electrode configuration measurement, the counter electrode was a Pt film (~160 nm) deposited on Ti foil by using direct current magnetron
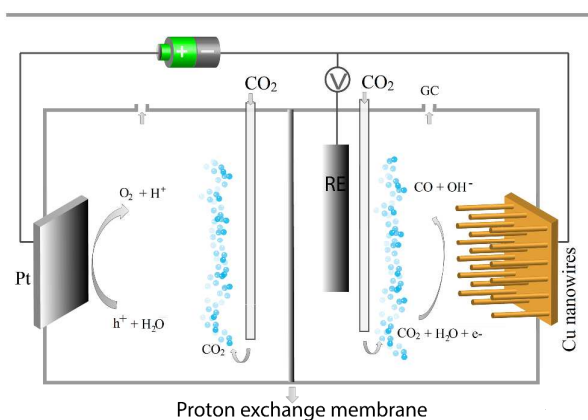
Fig. 1 The schematic illustration of the electrochemical cell used for reduction of CO_2

sputtering (XRD pattern of the Pt film sputtered on Ti foil is shown in Fig. S1) and an Ag/AgCl electrode (XR300, saturated KCl + AgCl solution (KS120), Radiometer Analytical) was used as the reference electrode (RE). The applied potentials vs. Ag/AgCl were converted to the reversible hydrogen electrode (RHE) using the equation:

$$V_{RHE} = V_{Ag/AgCl} + V^0_{Ag/AgCl \, vs \, NHE} + 0.059 pH \qquad (1)$$

where $V^0_{Ag/AgCl \, vs \, NHE}$ is 0.199 V at 25 °C. The electrochemical reduction of CO_2 was performed in a 0.1 M $KHCO_3$ (Sigma Aldrich, 99.95%) electrolyte saturated with CO_2 (pH = 6.83) at ambient temperature and pressure.

The cathodic compartment was continuously purged with a constant CO_2 flow rate and vented directly into the gas-sampling loop of a gas chromatograph (GC, Interscience) in order to enable periodic quantification of the gas-phase products. Liquid products formed during the CO_2 reduction were identified and quantified by nuclear magnetic resonance (NMR) after completion of the electrolysis.

2.5 NMR Data Analysis

NMR measurements were performed by an Agilent MR400DD2 NMR spectrometer operating at 400 MHz. Samples were prepared by mixing 450 µL of the electrolyte solutions with 50 µL of D2O containing internal reference t-BuOH with a known concentration. 1H NMR spectra were acquired by applying a hard pulse solvent pre-saturation pulse sequence with 2 s saturation delay, 2 s relaxation delay, 2.5 s acquisition time, and spectral window of 6400 Hz. Typically, 8 scans were collected and the peak areas were integrated in order to calculate the concentration of the solutes by taking into account the difference in the number of protons in the reference compound with respect to the product.

3. RESULTS AND DISCUSSION
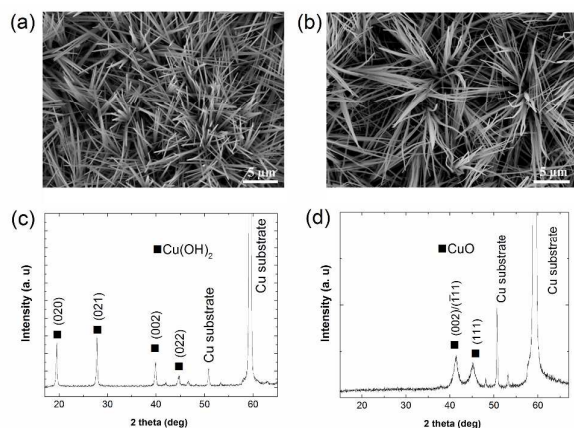
Fig. 2 SEM images and XRD patterns of $Cu(OH)_2$ nanowires before (a) (c) and after (b) (d) annealing in air at 150 ºC for 2 h, respectively.
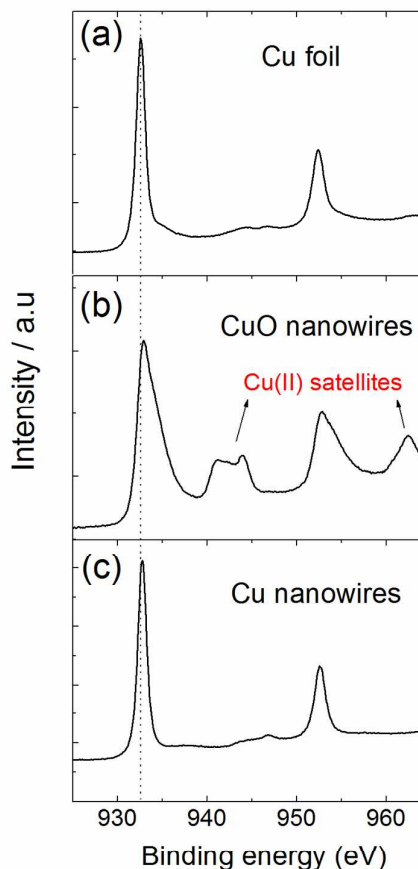
Fig. 3 XPS spectrum of the polycrystalline Cu foil (a) and CuO nanowires on Cu foil before (b) and after (c) CO_2 reduction electrolysis at -0.6 V vs. RHE.

3.1 Synthesis of CuO Nanowires

A typical SEM image of the prepared $Cu(OH)_2$ nanowires is shown in Fig. 2(a). The Cu substrate was uniformly covered with $Cu(OH)_2$ nanowires, which were observed to have an average diameter of around 100-250 nm and length of approximately 5-10 µm. The XRD pattern shown in Fig. 2(c) confirms the presence of $Cu(OH)_2$ in this sample, in addition to the presence of the Cu foil substrate. After this initial characterization, the $Cu(OH)_2$ nanowires were annealed to form CuO. The annealing temperature and time were adjusted to dehydrate the $Cu(OH)_2$ nanowires in air and argon, respectively (shown in Fig. S3), and the optimal conditions were found to be 150 ºC for 2 hours in an air atmosphere. While the copper oxide nanowires retained their nanostructured morphology after annealing, a slight bundling of the nanowires was observed, as shown in Fig. 2 (b). The XRD pattern in Fig. 2 (d) reveals the $Cu(OH)_2$ nanowires were dehydrated to form CuO after annealing in air at 150 ºC for 2 hours, with no more indication of any remaining $Cu(OH)_2$.

3.2 CuO-derived Cu Nanowires

The resulting CuO nanowire arrays were directly utilized in electrochemical reduction of CO_2 in CO_2-saturated 0.1 M $KHCO_3$ electrolytes, and were reduced to Cu nanowires during electrolysis. In order to confirm the formation of the Cu nanowires, further characterization of the samples was performed. The SEM images of CuO nanowires after CO_2 reduction electrolysis at -0.6 V vs. RHE reveals the nanowires structure, as shown in Fig. S4, therefore we conclude that all CO_2 electrochemical reduction experiments occurred on nanowire structured substrates.

To confirm the oxidation states of the samples before and after CO_2 reduction, XPS measurements were performed. The Cu 2p XPS spectrum of the polycrystalline Cu foil (before CO_2 reduction electrolysis) and the CuO nanowires on the Cu foil substrate before and after CO_2 reduction electrolysis are shown in Fig. 3. The Cu $2p_{3/2}$ peak at 932.58 eV was observed for the polycrystalline Cu foil, shown in Fig. 3 (a). For the CuO nanowire sample, the Cu $2p_{3/2}$ peak shifted to a higher binding energy (932.98 eV) and was much broader compared to that of Cu foil, which is consistent with the Cu $2p_{3/2}$ peak analysis of CuO and Cu in previous reports.[35] In addition to the shift of the Cu $2p_{3/2}$ peak between CuO and Cu, the Cu oxidation states can be further distinguished by observing satellite features in the Cu2p XPS spectrum.[35] Cu^{2+} satellite peaks at 941.3, 943.9 and 962.5 eV in Fig. 3 (b) indicate the presence of CuO, which is consistent with the observation from the XRD pattern shown in Fig. 2 (d). After CO_2 reduction electrolysis, the Cu $2p_{3/2}$ peak shifted back to a lower binding energy of 932.78 eV, and the Cu^{2+} satellite peaks were no longer observed, as shown in Fig. 3 (c), indicating the presence of Cu^0 or Cu^{1+} after CO_2 reduction. The Cu 2p XPS spectrum of the nanowires after CO_2 reduction is almost identical to that of the polycrystalline Cu foil. In addition, we only observed Cu^0 peaks in the XRD pattern of the nanowires after CO_2 reduction electrolysis (Fig. S5). These data indicate that the CuO nanowires in this study were reduced to Cu during the electrochemical reduction of CO_2. Thus, we can confirm that the electrochemical reduction of CO_2 in our study occurred on Cu nanowire arrays.

3.3 CO_2 Reduction Performance on CuO-derived Cu Nanowires

The electrocatalytic CO_2 reduction results on Cu nanowires and Cu foils are presented in Fig. 4. It was found that the Cu nanowire array electrodes exhibited an initial high geometric current density (for instance, Fig. S8 shows $j_{tot} > 1$ mA/cm^2 for 390 seconds at -0.6 V vs. RHE) as the CuO nanowires were reduced to Cu nanowires, and subsequently a stable current density was observed during electrolysis. At a negative potential of -0.35 V vs. RHE, the Cu nanowire arrays revealed a stable j_{tot} with a FE of ~ 18% for CO production. At a more negative potential of -0.5 V vs. RHE, Cu nanowire arrays exhibited an increased j_{tot} in Fig. 4 (b), and a FE of ~ 30% for CO and a FE of ~ 7.5% for HCOOH (Fig. 5) were observed. Notably, a peak FE of ~ 50% for CO production (the FE for HCOOH was ~ 30% in Fig. 5) on Cu nanowires was reached at -0.6 V vs. RHE shown in Fig. 4 (a), corresponding to an overpotential of 490 mV relative to the CO_2/CO equilibrium potential (-0.11 V vs.
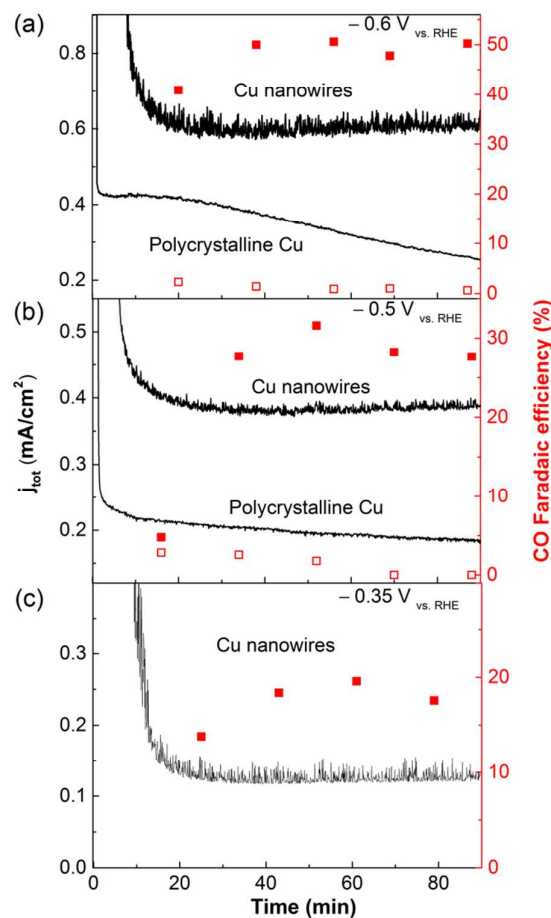
Fig. 4 CO_2 reduction performance of CuO-derived Cu nanowires. CO_2 reduction activity of CuO-derived Cu nanowires and polycrystalline Cu foil at (a) -0.6 V and (b) -0.5 V, and CuO-derived Cu nanowires at (c) -0.35 V vs. RHE in CO_2-saturated 0.1 M $KHCO_3$ electrolytes (no CO production was observed for polycrystalline Cu at -0.35 V vs. RHE). The geometric current density is shown on the left axis and the faradaic efficiency for CO is shown on the right axis (■ and □ represent CO faradaic efficiency on Cu nanowires and Cu foil respectively).

RHE). Furthermore, a relatively stable FE for CO production on Cu nanowire arrays was observed in Fig. 4, indicating the catalytic activity for CO_2 reduction on Cu nanowire arrays was relatively stable during that time.

In contrast, the polycrystalline Cu electrodes experienced a decrease in current density over time under identical conditions, as shown in Fig. 4 (a, b). In addition, the polycrystalline Cu substrates showed a low faradaic efficiency for CO (FE < 3% at -0.5 V and -0.6 V vs. RHE), and the FE for CO decreased over time shown in Fig. 4 (a, b), which indicates a fast decrease in catalytic activity for CO_2 reduction. It was found that the FE for HCOOH on the polycrystalline Cu foils was only ~11.6% at -0.6 V vs. RHE (Fig. 5). It was reported that the performance of CO_2 reduction on polycrystalline Cu foil in electrolytes without stringent purification could not be observed due to rapidly complete deactivation of catalytic activity.[18,28] Indeed, in our study, at less negative potentials
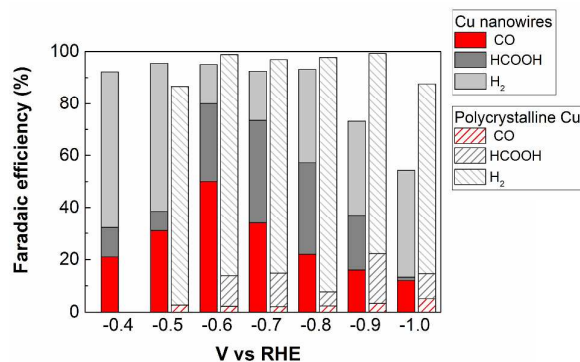
Fig.5 Faradaic efficiency for CO, HCOOH and H$_2$ at various potentials in CO$_2$-saturated 0.1 M KHCO$_3$ electrolytes at ambient temperature and pressure.

than -0.5 V vs. RHE, the CO production on polycrystalline Cu did not reach the detection limit of our GC.

CO$_2$ reduction on Cu nanowire arrays and Cu foils was also performed at more negative potentials in order to investigate the FE for products (HCOOH, CO and H$_2$) as a function of potentials, as shown in Fig. 5. The FE for CO on Cu nanowire arrays obviously increased with increasing overpotentials at potentials of ≥ -0.6 V vs. RHE and then evidently declined with further increasing overpotentials at potentials of ≤ -0.6 V vs. RHE. Similarly, the FE for formic acid on Cu nanowire arrays also experienced an increase at potentials of ≥ -0.7 V vs. RHE and a decrease at potentials of ≤ -0.7 V vs. RHE. It can be readily found that highest FE of ~ 50% for CO production on Cu nanowire arrays was obtained at -0.6 V vs. RHE, while the peak FE of ~ 40% for HCOOH on Cu nanowire arrays was reached at a more negative potential (-0.7 V vs. RHE).

Because H$_2$ evolution is always a competing reaction with CO$_2$ reduction in CO$_2$-saturated electrolytes, H$_2$ was also identified and quantified as a function of potentials during CO$_2$ reduction electrolysis shown in Fig. 5. As we note in Fig. 5, the total faradaic efficiencies for all the reduction products of CO$_2$ (the FE for CO is ~ 50% and the FE for HCOOH is ~ 30%) on Cu nanowire arrays add up to ~ 80% at -0.6 V vs. RHE. Only 15% FE for H$_2$ is produced on Cu nanowire arrays at this potential. As a comparison, the majority of the current on the polycrystalline Cu foils is used for H$_2$ evolution at various potentials (Fig. 5), which is consistent with previous studies for Cu foil in CO$_2$-saturated electrolytes.[6,18]

At less negative potentials (-0.4 V and -0.5 V vs. RHE), the decrease in total faradaic efficiencies for CO and HCOOH on Cu nanowire arrays corresponds to an increase of faradaic efficiency for H$_2$ evolution with lower overpotentials, as shown in Fig. 5, which is attributed to the fact of that the overpotential is not high enough to drive CO$_2$ reduction efficiently which is directly competing with H$_2$ evolution that requires a relatively small overpotential to occur.[5] At more negative potentials than -0.6 V vs. RHE, the total faradaic efficiencies for CO and HCOOH decreases with increasing overpotentials and the corresponding faradaic efficiency for H$_2$ evolution increases. Furthermore, hydrocarbon gas phase

products (ethylene and ethane) are observed at more negative potentials (-0.8 V, -0.9 V and -1.0 V vs. RHE) in Fig. S9. At more negative potentials, the rate of CO$_2$ reduction (μmol/s/cm^2) shows a dramatic increase up to ~ -0.7 V vs. RHE, and then increases much slower with increasing potentials (shown in Fig. S10), which indicates mass transfer limitations at higher overpotentials.[18] Thus, with more negative potentials (< -0.6 V vs. RHE), the observed decrease in the total faradaic efficiencies for CO$_2$ reduction and the increase in faradaic efficiency for H$_2$ evolution reflect the mass transport limitations at relatively high current densities.[18]

3.4 Enhanced Performance Mechanism

The surface roughness factor for the Cu nanowires arrays relative to polycrystalline Cu foils were determined by measuring the electrochemical double-layer capacitance.[28,33,34] In Fig. S6, Cu nanowire arrays show a capacitance of 3.5 mF, which means that the surface roughness factor is ~ 80 times larger than that of the smooth polycrystalline Cu foil (the capacitance of 0.043 mF in Fig. S7). Thus, the increase of the geometric current density (Fig. 4) for Cu nanowire arrays during the electrochemical reduction of CO$_2$ can be explained taking into account the higher surface area of the Cu nanowire arrays. Furthermore, the high catalytic selectivity (high FE for CO and HCOOH) for CO$_2$ reduction on Cu nanowire arrays may be attributed to the high surface area of Cu nanowire arrays that may provide more active sites for CO$_2$ reduction electrolysis. It is interesting to note, however, the roughness factor difference (~ 80×) is considerably larger than the difference in j$_{tot}$ between the two electrodes (~ 2×). The discrepancy between the increased surface area and increased j$_{tot}$ seems to show that all of the increased surface area is not active for CO$_2$ reduction. One possible mechanism is the coverage of active CO$_2$ reduction sites caused by product formation, where the reaction products block active sites. This coverage of active sites is most likely to reduce the overall efficiency, because the long length of the nanowires may make product diffusion very difficult.

In order to compare the catalytic activity, cyclic voltammetry of Cu nanowires and smooth Cu in CO$_2$-saturated 0.1 M KHCO$_3$ electrolytes were shown in Fig. S12. The
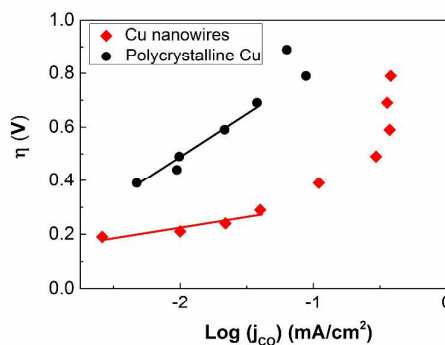
Fig. 6 Tafel plots of the CO partial current density for polycrystalline Cu and Cu nanowires.
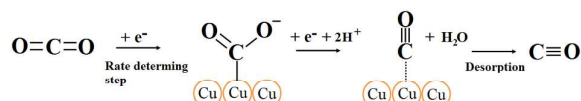
Fig. 7 Proposed mechanism for reduction of CO_2 to CO on metals.[6,21]

corresponding potentials at the electroreduction current density of 0.5 mA/cm^2 for smooth Cu and Cu nanowires are observed at -0.69 V and -0.51 V vs. RHE, respectively. This positive shift from -0.69 V to -0.51V may indicate the improved catalytic activity for CO_2 reduction on Cu nanowire arrays.

Further insight into the kinetics of CO_2 reduction on catalysts can be examined by a Tafel plot analysis.[5,18,9,17] Here, a Tafel plot of Cu nanowire arrays (overpotential versus log of the partial current density for CO production) is shown in Fig. 6. Y. Hori has proposed that a two-electron transfer is involved in the electrochemical reduction of CO_2 to CO, as shown in Fig. 7.[6,21] In the initial step, a CO_2*^- intermediate adsorbed on metal surface is formed by a one-electron transfer to a CO_2 molecule.[6,9,21] Subsequently, the CO_2*^- on the surfaces takes two protons and one electron to form a CO and a H_2O molecule.[5,6,21] It is generally accepted that the first electron transfer for the formation of the CO_2*^- is the rate determining step for the whole process because the first electron transfer requires a much more negative potential compared to the following steps.[5]

A Tafel relationship between CO current i_{co} and overpotential η can be written as follows[36]:

$$i_{co} \propto P_{CO_2} \exp\left(\alpha \frac{F\eta}{RT}\right) \qquad (2)$$

where F is Faraday constant, R is the gas constant, T is the absolute temperature, P_{CO_2} is the partial pressure of CO_2, and α is the transfer coefficient.

From Henry's law, the concentration of the dissolved CO_2 in electrolytes can be expressed as

$$C_{CO_2} = KP_{CO_2} \qquad (3)$$

where K is constant. Then, equation (2) can be written as[36]:

$$i_{co} = nFkC_{CO_2} \exp\left(\alpha \frac{F\eta}{RT}\right) \qquad (4)$$

where n is the total number of electron transfer needed to convert CO_2 to CO, and k is the rate constant for converting CO_2 to CO (incorporating K)[36]. The Tafel slope is given by the partial derivative of the overpotential with respect to the log of the current. Thus, equation (4) can be rewritten as:

$$1 = \frac{\alpha F}{2.3RT}\left(\frac{\partial \eta}{\partial \log i_{co}}\right) \qquad (5)$$

According to the equation (5), the Tafel slope $\left(\frac{\partial \eta}{\partial \log i_{co}}\right)$ of ~110 mV/dec for Cu nanowire arrays (η < 0.3 V) shown in Fig. 6 corresponds to the transfer coefficient of 0.54, which is consistent with the concept that the rate determining step of

the reaction is the initial electron transfer to CO_2 on metal electrodes.[6] According to previous studies[5,9,17,18], the low Tafel slope indicates a fast initial electron transfer to a CO_2 molecule (the rate determining step), which implies that the formation of the adsorbed CO_2*^- intermediate may be favored on Cu nanowire arrays. Therefore, according to these results, it appears that CuO-derived Cu nanowires are able to provide the enhanced stabilization for the CO_2*^- intermediate.

4. Conclusions

In summary, CuO-derived Cu nanowire array electrodes prepared by a simple method were capable of reducing CO_2 selectively to CO and HCOOH with high faradaic efficiencies (~ 50% and ~30%, respectively) at a moderate potential of -0.6 V vs. RHE (η_{CO} = 490 mV and η_{HCOOH} = 410 mV, respectively). This high faradaic efficiency for CO_2 reduction may be due to the more active sites on the high surface area of Cu nanowires, and the high catalytic selectivity for the reduction of CO_2 to CO is attributed to the dramatically enhanced stabilization for the CO_2*^- intermediate. This study shows the surface morphology of Cu electrocatalysts could dramatically influence the catalytic selectivity for CO_2 reduction, making them an excellent platform for future studies of electrochemical reduction of CO_2.

Acknowledgements

References

1   S. J. Davis, K. Caldeira and H. D. Matthews, *Science*, 2010, **329**, 1330–1333.
2   J. M. Hall-Spencer, R. Rodolfo-Metalpa, S. Martin, E. Ransome, M. Fine, S. M. Turner, S. J. Rowley, D. Tedesco and M.-C. Buia, *Nature*, 2008, **454**, 96–99.
3   R. S. Haszeldine, *Science*, 2009, **325**, 1647–1652.
4   D. T. Whipple and P. J. a. Kenis, *J. Phys. Chem. Lett.*, 2010, **1**, 3451–3458.
5   Q. Lu, J. Rosen, Y. Zhou, G. S. Hutchings, Y. C. Kimmel, J. G. Chen and F. Jiao, *Nat. Commun.*, 2014, **5**, 3242.
6   Y. Hori, in *Modern Aspects of Electrochemistry*, ed. C. G. Vayenas, Springer New York, 2008, pp 89–189.
7   K. P. Kuhl, E. R. Cave, D. N. Abram and T. F. Jaramillo, *Energy Environ. Sci.*, 2012, **5**, 7050–7059.
8   J. Qiao, Y. Liu, F. Hong and J. Zhang, *Chem. Soc. Rev.*, 2014, **43**, 631–675.
9   M. Gattrell, N. Gupta and A. Co, *J. Electroanal. Chem.*, 2006, **594**, 1–19.

10 S. Sen, D. Liu and G. T. R. Palmore, *ACS Catal.*, 2014, **4**, 3091–3095.

11 O. A. Baturina, Q. Lu, M. A. Padilla, L. Xin, W. Li, A. Serov, K. Artyushkova, P. Atanassov, F. Xu, A. Epshteyn, T. Brintlinger, M. Schuette and G. E. Collins, *ACS Catal.*, 2014, **4**, 3682–3695.

12 C. H. Lee and M. W. Kanan, *ACS Catal.*, 2015, **5**, 465–469.

13 Y. Zhang, V. Sethuraman, R. Michalsky and A. A. Peterson, *ACS Catal.*, 2014, **4**, 3742–3748.

14 K. J. P. Schouten, E. Pérez Gallent and M. T. M. Koper, *ACS Catal.*, 2013, **3**, 1292–1295.

15 D. J. Wilhelm, D. R. Simbeck, a. D. Karp and R. L. Dickenson, *Fuel Process. Technol.*, 2001, **71**, 139–148.

16 Y. Chen and M. W. Kanan, *J. Am. Chem. Soc.*, 2012, **134**, 1986–1989.

17 Y. Chen, C. W. Li and M. W. Kanan, *J. Am. Chem. Soc.*, 2012, **134**, 19969–19972.

18 C. W. Li and M. W. Kanan, *J. Am. Chem. Soc.*, 2012, **134**, 7231–7234.

19 T. Hatsukade, K. P. Kuhl, E. R. Cave, D. N. Abram and T. F. Jaramillo, *Phys. Chem. Chem. Phys.*, 2014, **16**, 13814–13819.

20 D. Plana, J. Flórez-Montaño, V. Celorrio, E. Pastor and D. J. Fermín, *Chem. Commun. (Camb).*, 2013, **49**, 10962–10964.

21 Y. Hori, H. Wakebe, T. Tsukamoto and O. Koga, *Electrochim. Acta*, 1994, **39**, 1833–1839.

22 Y. Hori, H. Wakebe, T. Tsukamoto and O. Koga, *Surf. Sci.*, 1995, **335**, 258–263.

23 K. J. P. Schouten, Z. Qin, E. Pérez Gallent and M. T. M. Koper, *J. Am. Chem. Soc.*, 2012, **134**, 9864–9867.

24 F. Calle-Vallejo and M. T. M. Koper, *Angew. Chemie*, 2013, **125**, 7423–7426.

25 Y. Hori, K. Kikuchi and S. Suzuki, *Chem. Lett.*, 1985, 1695–1698.

26 Y. Hori, K. Kikuchi, A. Murata and S. Suzuki, *Chem. Lett.*, 1986, 897–898.

27 R. Reske, H. Mistry, F. Behafarid, B. Roldan Cuenya and P. Strasser, *J. Am. Chem. Soc.*, 2014, **136**, 6978–6986.

28 R. Kas, R. Kortlever, A. Milbrat, M. T. M. Koper, G. Mul and J. Baltrusaitis, *Phys. Chem. Chem. Phys.*, 2014, **16**, 12194–201.

29 W. Tang, A. a Peterson, A. S. Varela, Z. P. Jovanov, L. Bech, W. J. Durand, S. Dahl, J. K. Nørskov and I. Chorkendorff, *Phys. Chem. Chem. Phys.*, 2012, **14**, 76–81.

30 Xie, Y. Huang and H. Yu, Front. Environ. Sci. Eng., 2014, 1–6.

31 W. Zhang, X. Wen, S. Yang, Y. Berta and Z. L. Wang, *Adv. Mater.*, 2003, **15**, 822–825.

32 C. Lin, Y. Lai, D. Mersch and E. Reisner, *Chem. Sci.*, 2012, **3**, 3482–3487.

33 C. C. L. McCrory, S. Jung, J. C. Peters and T. F. Jaramillo, *J. Am. Chem. Soc.*, 2013, **135**, 16977–16987.

34 C. W. Li, J. Ciston and M. W. Kanan, *Nature*, 2014, **508**, 504–507.

35 M. C. Biesinger, L. W. M. Lau, A. R. Gerson and R. S. C. Smart, *Appl. Surf. Sci.*, 2010, **257**, 887–898.

36 Y. Hori and S. Suzuki, *J. Electrochem. Soc.*, 1983, **130**, 2387-2390.